

Check for updates

Gram-Scale Green-Synthesis of High Purity Pinacols and Amides by Continuous Tandem Photocatalysis via a **Negative Carbon Emission Process**

Xiao-Liang Ma, Wen-Xiong Shi, Song Guo, * Qiu-Ping Zhao, Wenbin Lin, Tong-Bu Lu, * and Zhi-Ming Zhang*

Solar-driven CO₂ reduction for practical applications confronts significant challenges, including the waste of oxidation power and the difficulty in isolating reduction products. Herein, a pre-coordination restriction strategy is presented to hierarchically assemble CdS quantum dots (QDs), cobalt sites and Zr₆ clusters in one metal-organic framework (MOF), resulting in the CdS@PCN-Co composite for simultaneous CO2 photoreduction and C-C coupling. Impressively, the yields of CO and pinacols with CdS@PCN-Co can reach 59.5 mmol·g⁻¹ (99.4% selectivity) and 56.2 mmol·g⁻¹ (95.3% selectivity), respectively, over six and seven times higher than those with the CdS/PCN-Co mixture (9.8 mmol • g⁻¹ CO, 29.4% selectivity; 7.8 mmol • g⁻¹ pinacols, 22.7% selectivity). The superior catalytic performance of CdS@PCN-Co can be ascribed to the synergy among encapsulated CdS QDs, Zr₆ clusters and PCN-Co, where photogenerated electrons can efficiently transfer from CdS QDs to Co sites for selective CO generation while the remaining holes can oxidize the adsorbed 1-phenylethanol over Zr₆ surface to facilitate C-C coupling. More impressively, the released CO can be immediately used for carbonylation photosynthesis by immobilizing CdS@PCN-Co and Pd/PCN-Zn in a continuous-flow system with two reactors, which simultaneously achieves gram-scale photosynthesis of high-purity pinacols and amides by continuous tandem photocatalysis.

1. Introduction

The substantial consumption of fossil fuel in traditional industrial processes results in excessive carbon dioxide (CO₂)

X.-L. Ma, W.-X. Shi, S. Guo, Q.-P. Zhao, T.-B. Lu, Z.-M. Zhang State Key Laboratory of Crystal Materials Institute for New Energy Materials and Low Carbon Technologies School of Materials Science & Engineering Tianjin University of Technology Tianjin 300384, China E-mail: guosong@email.tjut.edu.cn; lutongbu@tjut.edu.cn; zmzhang@email.tjut.edu.cn W. Lin Department of Chemistry The University of Chicago

Chicago, IL 60637, USA

The ORCID identification number(s) for the author(s) of this article can be found under https://doi.org/10.1002/adma.202506133

DOI: 10.1002/adma.202506133

emissions, which exacerbate the energy crisis and environmental issues.[1-7] Solardriven CO2 reduction into fuels has been regarded as one of the most promising strategies to simultaneously reduce fossil fuel consumption and lower atmospheric CO2 concentrations.[8-19] In this regard, photocatalysts play a crucial role in light absorption, charge separation/transfer, and catalytic conversion in the photocatalytic process, significantly influencing the performance of CO₂ reduction.[20-24] Metalorganic frameworks (MOFs), with their structurally designable ligands, pores, and metal nodes, serve as a versatile molecular platform to develop efficient photocatalysts for CO₂ reduction.^[23,25–35] Despite considerable advancements, current catalytic systems primarily convert CO2 into various C1 products, such as CO and HCOOH, with low yields within the nanomolar to micromolar range.[36-39] Additionally, when the photogenerated electrons are used for CO₂ reduction, the accompanying holes are typically consumed by sacrificial agents, such as trimethylamine (TEA),

triethanolamine (TEOA), or 1,3-dimethyl-2-phenyl-2,3-dihydro-1H-benzo[d]imidazole (BIH).[40,41] Therefore, the waste of photogenerated holes, along with the low value of C1 products, significantly restricts their practical applications. To promote the industrialization of CO2 photoreduction, the following challenges are urgent to be addressed: i) Upcycling products of CO2 reduction into value-added chemicals, ii) High value-added utilization of oxidation power, iii) Developing sustainable catalytic systems to integrate processes (i, ii), and CO₂ photoreduction. [22,42,43]

To achieve the above goals, it is essential to develop a novel catalytic system that is compatible with three key processes: light-induced oxidative organic synthesis, [44-46] CO₂ photoreduction, [47] and carbonylation reactions using CO as a C1 source. [48] However, conventional one-pot photocatalytic systems using a photocatalyst make it difficult to integrate these reaction processes due to their conflicting reaction conditions (Figure 1a). Recently, pioneering attempts have been made for tandem catalysis with a dual-chamber reactor to couple CO₂-to-CO conversion with carbonylation reactions.^[24,49–58] In these catalytic systems, the conversion of CO2 to CO has

15214095, 0, Downloaded from https://advanced.onlinelibrary.wiley.com/doi/10.1002/adma.202506133 by Tianjin University Of, Wiley Online Library on [1407/2025]. See the Terms

onditions) on Wiley Online Library for rules of use; OA articles are governed by the applicable Creative Common

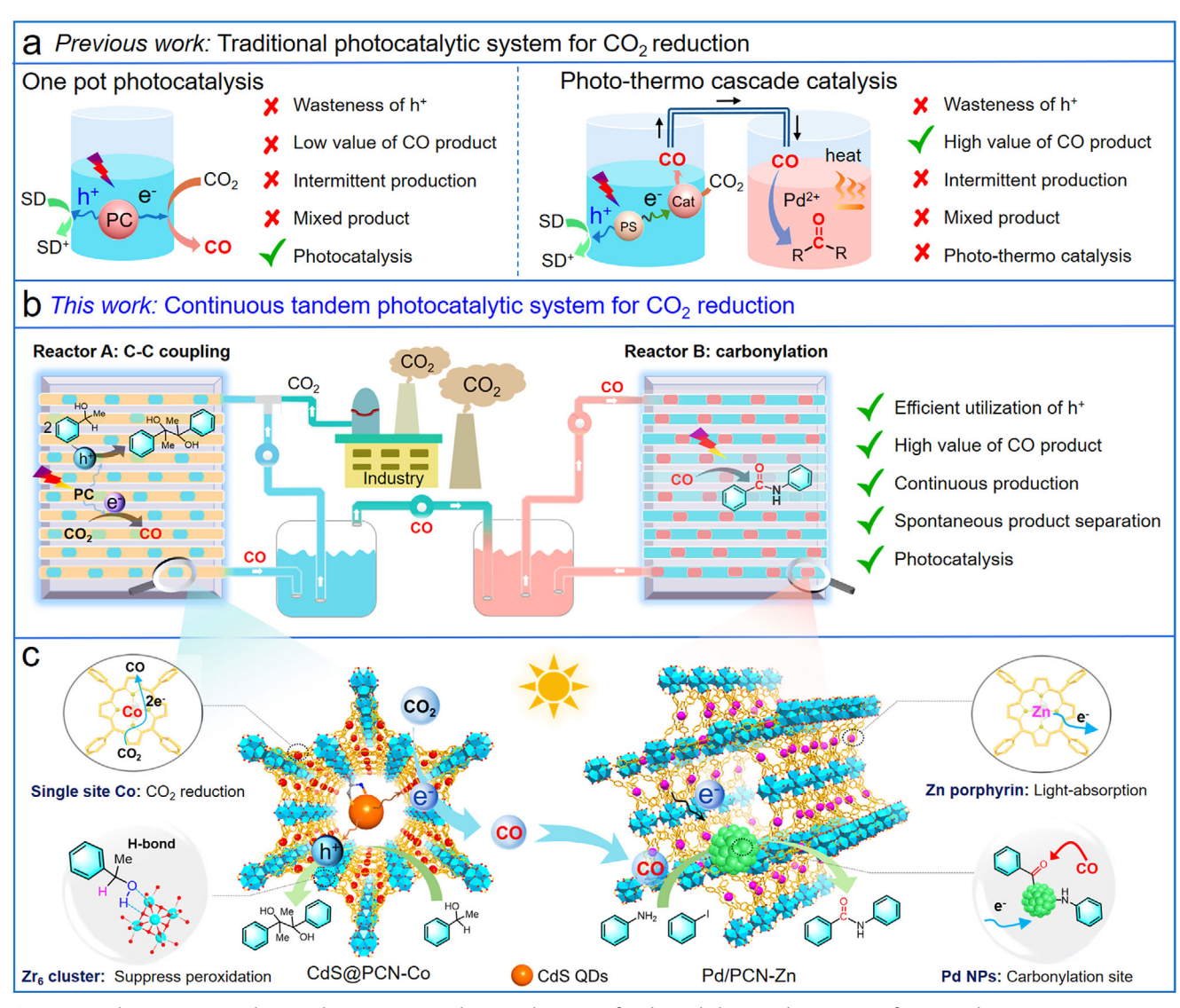


Figure 1. Tandem continuous photocatalytic system. a) Schematic diagrams of traditional photocatalysis systems for CO₂ reduction containing one pot photocatalysis and photo-thermo cascade catalysis. b) Tandem continuous-flow reactors for simultaneous C–C coupling and photocatalytic carbonylation mediated by photochemical CO₂-to-CO reduction. c) Photocatalytic CO₂-to-CO reduction coupled with oxidative organic synthesis by CdS@PCN-Co and subsequent utilization of CO for photocatalytic carbonylation catalyzed by Pd/PCN-Zn. PC: photocatalyst. PS: photosensitizer. Cat: catalyst. QDs: quantum dot. NPs: nanoparticles.

been achieved through electrocatalytic,^[51] photocatalytic,^[49,50] and fluoride-catalytic strategies,^[52] then the produced CO was used to feed carbonylation reactions via a conventional thermal catalysis process. For instance, Lan et al. employed [Ru(bpy)₃]Cl₂ as a sensitizer, TEOA as an electron donor, and NNU-55-Ni as a catalyst for photoreduction of CO₂ to CO.^[59] Subsequently, CO was used as a C1 source for thermalcatalytic carbonylation reactions. Audisio et al. utilized [Ru(bpy)₃]Cl₂ as a sensitizer, BIH as an electron donor, and rhenium-based complex as a photocatalyst for the reduction of radioisotope-tagged ¹¹CO₂ and ¹⁴CO₂. The resulting ¹¹CO and ¹⁴CO can serve as C1 feedstocks for the synthesis of isotopically labeled carbonyl-containing drug molecules.^[54] These photocatalytic systems are usually constrained by the following factors: inefficient utilization of photogenerated holes, reliance on external photosensitizers, intermittent product for

mation, mixed product, and excessive thermal consumption. To our knowledge, the concurrent value-added utilization of oxidation power and CO_2 reduction products has not yet been realized. Therefore, it's highly desirable but remains a great challenge to achieve sustainable photosynthesis through a negative carbon emission process by simultaneously developing photocatalysts and photocatalytic systems.

Herein, we developed a pre-coordination restriction strategy to hierarchically assemble CdS quantum dots (QDs), cobalt sites, and Zr $_6$ clusters within a single MOF matrix, resulting in the CdS@PCN-Co composite for simultaneous CO $_2$ photoreduction and C–C coupling. The encapsulated CdS QDs can denote photogenerated electrons to Co sites for CO $_2$ -to-CO conversion, while the remaining holes can oxidize 1-phenylethanol on Zr $_6$ surface to facilitate C–C coupling to produce pinacols with a 95.3%

15214095, 0, Downloaded from https://advanced.onlinelibrary.wiley.com/doi/10.1002/adma.202506133 by Tianjin University Of, Wiley Online Library on [14.07/2025]. See the Terms and Conditions (https://onlinelibrary.wiley

on Wiley Online Library for rules of use; OA articles are governed by the applicable Creative Commons

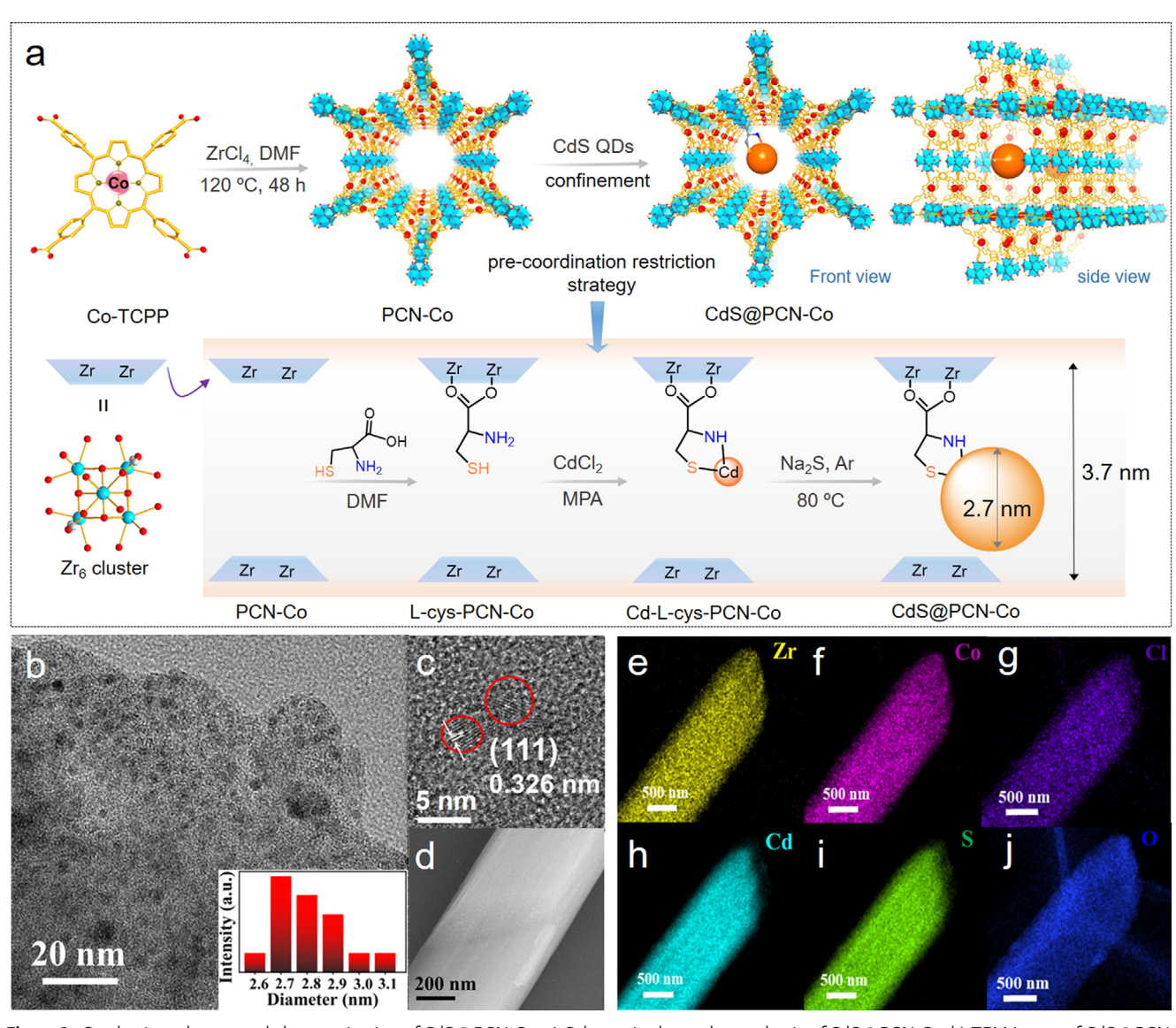


Figure 2. Synthesis and structural characterization of CdS@PCN-Co. a) Schematic shows the synthesis of CdS@PCN-Co. b) TEM image of CdS@PCN-Co. Inset: lattice spacing of CdS QDs. c) HRTEM image, d) scanning electron microscopy (SEM) image and e-j) elemental mapping images of CdS@PCN-Co.

selectivity. Impressively, CO yield can reach 59.5 mmol•g⁻¹ with 99.4% selectivity, nearly six times higher than those with the CdS/PCN-Co mixture (9.8 mmol • g⁻¹ CO, 29.4% selectivity), representing a record performance among all the visible-light absorbing MOF catalysts. Subsequently, we developed a tandem catalytic system consisting of dual continuous-flow reactors (A and B, Figure 1b) with dual MOF photocatalysts to integrate CO₂ photoreduction with photo-oxidative C-C coupling and photocatalytic carbonylation. Remarkably, gram-scale photosynthesis of pinacol was successfully achieved accompanied by efficient CO evolution, when immobilizing CdS@PCN-Co in reactor A. Then the released CO was directly pumped into reactor B, where Pd/PCN-Zn catalyzed its conversion to the commercial pesticide DEET (N,N-diethyl-3-methylbenzamide) with 98% selectivity (Figure 1c). For the first time, gram-scale greensynthesis of high-purity pinacols and amides was achieved by continuous tandem photocatalysis via a negative carbon emission process.

2. Results and Discussion

2.1. Synthesis and Characterization

PCN-Co/Zn of PCN-222 (PCN) were synthesized via a hydrothermal reaction of Co/Zn-TCPP (TCPP = tetrakis(4-carboxyphenyl)porphyrin) and ZrCl₄ at 120 °C (**Figure 2a**; Schemes S1–S3, Supporting Information). After immobilizing *L*-cysteine (L-cys) onto the Zr₆ nodes, CdS QDs were encapsulated in the L-cys modified PCN-Co (L-cys-PCN-Co) via a double-solvent approach. In this synthesis, the L-cys groups lining the MOF channels bound cadmium ions and then reacted with Na₂S to form CdS QDs in the confinement space, leading

15214095, D. Dwwloaded from https://advanced.onlinelibrary.wiley.com/doi/10.1002/adma.202506133 by Tanjan University Of, Wiley Online Library on [1407/2025]. See the Terms and Conditions (https://onlinelibrary.wiley.com/terms-and-conditions) on Wiley Online Library for rules of use; OA articles are governed by the applicable Cerative Commons

to the CdS@PCN-Co composite (Scheme S4, Supporting Information). For comparison, we also synthesized the CdS/PCN-Co control through the growth of CdS QDs on the external surface of PCN-Co in an aqueous environment^[62] and the CdS@PCN control by omitting the Co centers (Scheme S5, Supporting Information). The deposition of Pd NPs onto the surface of PCN-Zn was achieved by introducing K_2 PdCl₄ into a dispersion of the PCN-Zn MOF in water and ethanol. This mixture was subsequently reduced by using sodium borohydride, resulting in the formation of Pd/PCN-Zn (Scheme S6, Supporting Information). All these MOF samples were systematically characterized (Figures S1–S27 and Tables S1 and S2, Supporting Information).

Powder X-ray diffraction (PXRD) patterns of L-cys-PCN, Lcys-PCN-Co, and Pd/PCN-Zn matched well with the simulated PXRD pattern based on the crystal data of PCN, and the peaks at 5.2° were attributed to the (001) diffraction (Figure S20, Supporting Information). In addition to the PXRD peaks for PCN, CdS@PCN-Co, CdS@PCN, and CdS/PCN-Co all showed weak and broad diffraction peaks at ≈26.5°, 44.0°, and 52.1°, which were assigned to the (111), (220), and (311) diffraction of CdS QDs. These results demonstrate the maintenance of the PCN framework after the introduction of L-cys, CdS QDs, Co centers, and Pd NPs (Figure \$20a,b, Supporting Information). Highresolution transmission electron microscopy (HRTEM) images showed the formation of CdS QDs with an average size of 2.8 ± 0.4 nm and a lattice fringe distance of 0.326 nm in CdS@PCN-Co (Figure 2b,c; Figure S21, Supporting Information). This lattice fringe distance corresponded to the (111) crystal face of CdS. Additionally, elemental mapping demonstrated uniform distributions of Zr, Co, Cd, S, N, O, and Cl elements in CdS@PCN-Co (Figure 2e-j; Figure S22, Supporting Information). These results support the successful immobilization of CdS QDs in CdS@PCN-Co. Unlike CdS@PCN-Co, CdS/PCN-Co showed the distributions of Cd and S elements mainly on the surface (Figure 2d; Figures S23 and S24, Supporting Information). While CdS@PCN-Co exhibited a smooth surface, CdS/PCN-Co showed the presence of numerous particles on the surface. These findings indicated that CdS QDs were primarily confined within the pores of CdS@PCN-Co but mainly distributed on the surface of CdS/PCN-Co.

Nitrogen sorption isotherms revealed that the Brunauer-Emmett-Teller surface area, pore volume, and pore size of CdS@PCN-Co were significantly reduced compared to L-cys-PCN-Co (Figure S28 and Table S3, Supporting Information), which further supports the encapsulation of CdS QDs in CdS@PCN-Co. Infrared spectra (IR) of PCN-Co, L-cys-PCN-Co, and CdS@PCN-Co were obtained to assess the interactions among L-cys, CdS, and PCN-Co (Figure \$29, Supporting Information). The characteristic stretching vibration peaks of Zr-OH and Zr-OH₂ were observed at 3672 and 2558 cm⁻¹ for PCN-Co. After the introduction of L-cys, these characteristic peaks become weaker due to the partial exchange of L-cys with OH⁻ and OH₂ on the Zr₆ cluster (Zr-OH / Zr-OH₂) (Figure S29a, Supporting Information). In addition, L-cys-PCN-Co exhibited the S-H stretching vibration peak at 2317 cm⁻¹, supporting the successful loading of L-cys in PCN-Co (Figure S29b, Supporting Information). After the introduction of CdS, the stretching vibration of the S-H bond almost disappeared. This can be ascribed to -SH undergoing deprotonation upon coordination with CdS.[63,64]

X-ray photoelectron spectroscopy (XPS) was used to investigate the valences of metal centers in CdS@PCN-Co and Pd/PCN-Zn (Figures \$30 and \$31, Supporting Information). The characteristic peaks of Co 2p_{3/2} and Co 2p_{1/2} were detected at 780.9 and 796.3 eV respectively, indicating the presence of the Co²⁺ site in CdS@PCN-Co (Figure \$30b, Supporting Information).[60] The valence state of Cd was determined as +2 according to the Cd $3d_{5/2}$ and Cd $3d_{3/2}$ binding energies of 405.0 and 411.7 eV, respectively (Figure S30c, Supporting Information). [65] In addition, the S 2p_{3/2} binding energies of 161.4 and 162.2 eV and the S 2p_{1/2} binding energies of 163.6 and 164.3 eV were attributed to the C-S and S-Cd moieties, respectively (Figure \$29c, Supporting Information). [66] These results indicate the strong interaction of L-cys and CdS QDs in CdS@PCN-Co. Furthermore, the distinct peaks at 335.6 and 341.0 eV correspond to the Pd $3d_{5/2}$ and Pd $3d_{3/2}$, respectively, indicating the presence of Pd 0 in Pd/PCN-Zn. $^{[60]}$ This confirmed the presence of Pd NPs in Pd/PCN-Zn (Figure S31, Supporting Information).

2.2. Photocatalytic CO₂ Reduction and C-C Coupling Reactions

CO₂ photoreduction experiments were conducted in the presence of 1-phenylethanol with CdS, PCN, CdS@PCN, CdS@PCN-Co, or CdS/PCN-Co as photocatalysts under visiblelightirradiation (≥400 nm, Figure 3a,b; Table S4, Supporting Information). CdS@PCN-Co gave a CO yield of 59.5 mmol•gand a CO selectivity of 99.4% under visible-light irradiation, which represents a record performance over previously reported photocatalysts (Table S5, Supporting Information). Simultaneously, 1-phenylethanol was efficiently transformed to pinacol via C-C coupling to achieve high pinacol yield and selectivity of 93.7% and 95.3%, respectively. With CdS QDs as the photocatalyst, the main products were H2 and acetophenone under the CO₂ atmosphere, with CO and pinacol selectivity of 35.8% and 30.4%, respectively. PCN-Co did not produce CO under identical conditions, indicating that PCN-Co cannot drive CO2 reduction in the presence of 1-phenylethanol. On the other hand, CdS@PCN mainly produced H₂ with CO and pinacol selectivity of 30.1% and 38.1%, respectively. These results confirm that all the components in CdS@PCN-Co are essential for efficient CO₂ reduction and C-C coupling reaction. It can be noted that the consumed ratio of excited electrons to holes was close to 1.0, indicating an electron-hole balance between photocatalytic CO₂ reduction and oxidative C-C coupling reactions. In addition, CdS@PCN-Co exhibited exceptional photochemical stability and was readily recycled and used in five runs without obvious loss in catalytic activity and product selectivity (Figure S32a, Supporting Information). The exceptional stability of CdS@PCN-Co was supported by PXRD, TEM, XPS, and inductively coupled plasma-mass spectrometry analyses (Figures S32–S35 and Table S6, Supporting Information). Under similar conditions, CdS QDs severely aggregated during the reaction (Figure \$36, Supporting Information). Isotopic labeling experiments were conducted using ¹³CO₂ as the C1 source, and only ¹³CO was observed by gas chromatography-mass spectrometry (Figure 3c). This result demonstrates that CO originates from CO₂ photoreduction.

15214095, 0, Downloaded from https://advanced.onlinelibrary.wiley.com/doi/10.1002/adma.202506133 by Tianjin University Of, Wiley Online Library on [14.07/2025]. See the Terms and Conditions (https://onlinelibrary.wiley.com/term

xonditions) on Wiley Online Library for rules of use; OA articles are governed by the applicable Creative Commons

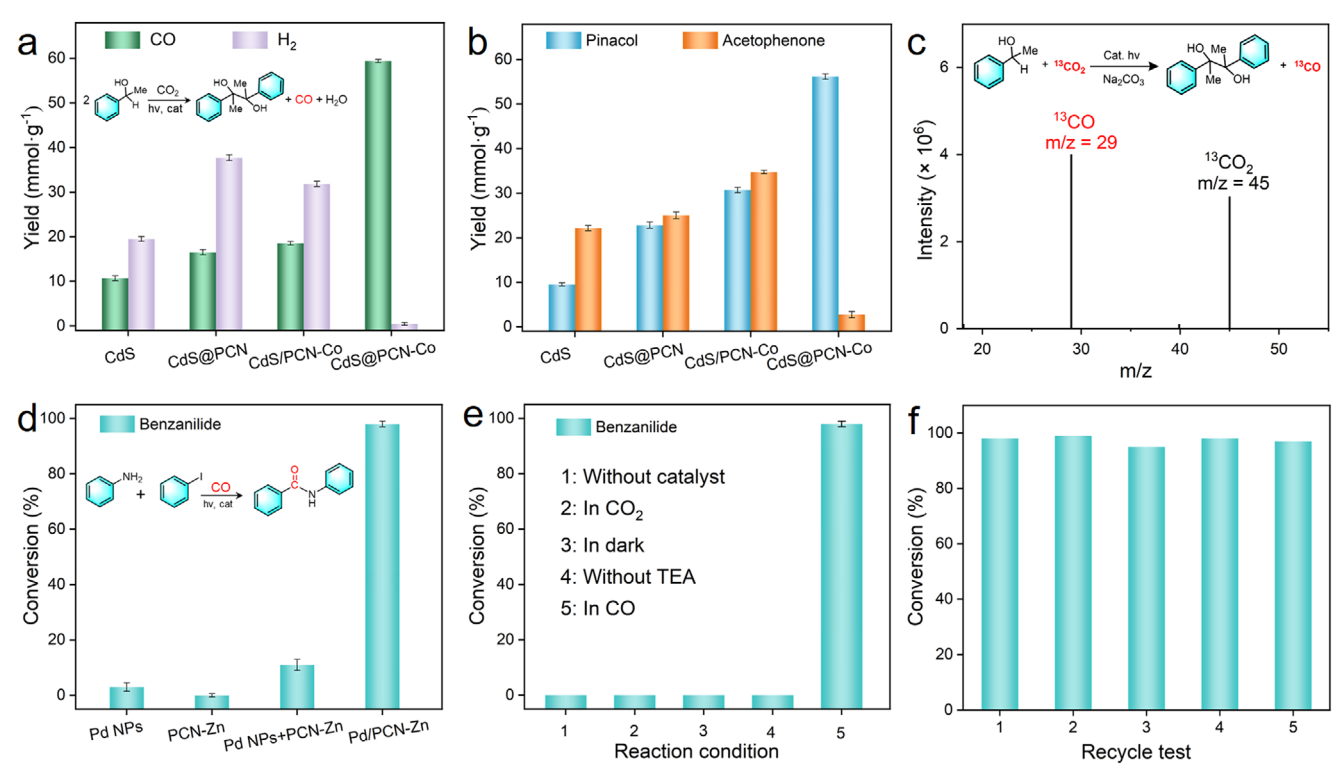


Figure 3. Catalytic performance for CO_2 photoreduction and carbonylation. a,b) Photocatalytic performance for CO_2 reduction and C–C coupling over CdS@PCN-Co. c) The isotope-tracing experiments of ^{13}CO (m/z=29) produced by photoreduction of $^{13}CO_2$ over CdS@PCN-Co. d) Photocatalytic performance for visible light-induced amino carbonylation reaction with different catalysts. e) Control photocatalytic experiments with Pd/PCN-Zn. f) Recycle experiments over Pd/PCN-Zn for visible light-induced amino carbonylation reaction.

We also examined the substrate scope and the effects of functional groups on C-C coupling reactions. 1-(paramethylphenyl)ethanol, 1-(p-methoxyphenyl)ethanol, 1-(pyridin-2-yl)ethanol, 1-phenyl-1-propanol, and 1-phenyl-1-butanol efficiently underwent photocatalytic reactions to reduce CO2 and generate pinacol derivatives (Table S7, Supporting Information). In these reactions, the CO yields ranged from 50.3 to 58.1 mmol•g⁻¹ with > 97.1% CO selectivity while the yields for pinacol derivatives exceeded 80% with > 93.0% selectivity. The substrates with electron-donating groups (-CH₃ and -OCH₃) at the p-positions of the aryl rings are tolerated in CO₂ reduction and C-C coupling reactions. However, the substrates with electronwithdrawing groups (-CF3 and -NO2) failed to drive the reaction, likely due to the difficulty of oxidative generation of the α hydroxybenzyl radicals by the photogenerated holes on CdS QDs. Interestingly, the substrates with -CH₃ and -OCH₃ substituents at the meta- and ortho-positions were oxidized to ketones instead of undergoing C-C coupling to form pinacols.

2.3. Photocatalytic Carbonylative Reaction with ¹²CO and ¹³CO₂ as C1 Source

The photocatalytic carbonylative reaction was conducted in a CO atmosphere upon irradiation with visible light. Remarkably, Pd/PCN-Zn can efficiently drive the carbonylative reaction to afford benzanilide with a yield of 98%. Only trace amounts of benzanilide were detected in the presence of Pd NPs or PCN-

Zn (Figure 3d). Moreover, the catalytic yield with the mixture of Pd NPs and PCN-Zn was determined to be 11%, much lower than that with Pd/PCN-Zn. This manifests that the close coupling between Pd NPs and PCN-Zn is necessary for efficient carbonylative reaction. In the absence of a catalyst, TEA or light, almost no product formed, suggesting that these factors are essential for carbonylation. When CO was replaced with CO₂, nearly no products were generated, indicating that Pd/PCN-Zn exclusively utilizes CO as a C1 source for carbonylation (Figure 3e). Furthermore, Pd/PCN-Zn can effectively facilitate the photosynthesis of DEET, a widely used commercial pesticide, achieving a yield of 99% (Figure \$37, Supporting Information). Additionally, Pd/PCN-Zn also exhibited superior photocatalytic stability, which can be recycled over five times without obvious loss of activity (>95%, Figure 3f). Isotopic tracing experiments were further performed in the tandem catalytic system under the ¹³CO₂ atmosphere. Notably, ¹³C-labeled benzoylaniline was obtained according to the analysis of high resolution mass spectrum results (Figure \$38, Supporting Information). This directly verifies the incorporation of ¹³C isotope labeling into the final product, thereby reinforcing the mechanism of the tandem system.

2.4. Photogenerated Carrier Separation and Electron Transfer

The roles of CdS QDs and Co sites upon light absorption and electron-hole separation in CdS@PCN-Co were investigated by steady-state and time-resolved spectroscopy and

15214095, D. Dwwloaded from https://advanced.onlinelibrary.wiley.com/doi/10.1002/adma.202506133 by Tanjan University Of, Wiley Online Library on [1407/2025]. See the Terms and Conditions (https://onlinelibrary.wiley.com/terms-and-conditions) on Wiley Online Library for rules of use; OA articles are governed by the applicable Cerative Commons

photoelectrochemical measurements. As shown in Figure S39a (Supporting Information), UV–vis absorption spectra exhibited an absorption band below 500 nm for CdS. After the introduction of CdS into PCN, CdS@PCN exhibited a broad absorption band between 300 and 800 nm with four Q bands at \approx 520, 555, 598, and 655 nm, which are present in the absorption spectra of PCN. In comparison, CdS@PCN-Co showed two Q bands, consistent with Co coordination to the porphyrin units of PCN. [60,67] Remarkably, both CdS@PCN-Co and Pd/PCN-Zn exhibited a strong and broadband visible light harvesting ability, highlighting their great potential for photosynthetic applications (Figure S39, Supporting Information).

Photoluminescence (PL) spectra were obtained to evaluate the electron-hole separation efficiency (Figure \$40, Supporting Information). As shown in Figure S40a (Supporting Information), CdS showed a strong PL emission peak at ≈600 nm, whereas PCN showed dual emissions at 670 and 725 nm. However, the PL of the CdS@PCN composite was significantly quenched compared to that of CdS and PCN. Furthermore, the PL signal of CdS@PCN-Co was nearly completely quenched after Co coordination. These results indicate that the separation efficiency of photogenerated electron-hole pairs follows the order of CdS@PCN-Co > CdS@PCN > PCN (or CdS). The rates of emission decay followed the trend of CdS@PCN-Co > CdS@PCN > PCN (or CdS), further supporting the most efficient photocarrier separation in CdS@PCN-Co among these samples (Figure S41a, Supporting Information). The photocurrent response of CdS@PCN-Co was much stronger than those of CdS@PCN and PCN (Figure S42, Supporting Information), whereas CdS@PCN-Co exhibited the smallest resistance among these photocatalysts (Figure S42b, Supporting Information). Additionally, the emission intensity of PCN-Zn was significantly quenched after introducing Pd NPs, manifesting an efficient electron transfer from PCN-Zn to Pd NPs (Figure S40b, Supporting Information). This viewpoint was further supported by photocurrent measurement, where the photocurrent intensity of Pd/PCN-Zn was remarkably higher than that of PCN-Zn (Figure S42c, Supporting Information). Additionally, the fluorescence lifetime of PCN-Zn was reduced from 1.8 to 1.1 ns for Pd/PCN-Zn, further confirming an electron transfer from PCN-Zn to Pd NPs (Figure S41, Supporting Information).

For CdS@PCN-Co, the conduction band (CB) and valence band (VB) of CdS QDs were determined as -0.66 and 1.49 V (vs NHE, pH 7), respectively (Figure \$43, Supporting Information). The higher CB potential of CdS QDs than that of PCN-Co provides the thermodynamic drive force for the transfer of photogenerated electrons from CdS QDs to the Co sites for CO2 reduction. Meanwhile, the VB potential of CdS QDs was more positive than the oxidation potential of 1-phenylethanol, indicating thermodynamic feasibility for 1-phenylethanol oxidation by the photogenerated holes on CdS QDs (Figures \$44 and S45a, Supporting Information). For Pd/PCN-Zn, upon irradiation with visible light, the excited Zn-porphyrin ligands can efficiently transfer electrons to Pd NPs, leading to the formation of electron-rich Pd NPs. This contributed to facilitating the carbonylation reaction (Figure S45b, Supporting Information).

2.5. Catalytic Mechanism

A series of control experiments and in situ electron paramagnetic resonance spectroscopic (EPR) studies were conducted to reveal the catalytic mechanism of CdS@PCN-Co (Figure 4; Figures S46–S52, Tables S8 and S9, Supporting Information). With the addition of AgNO3 as an electron scavenger, CdS@PCN-Co produced pinacol in relatively high activity but failed to generate CO. The addition of TEOA as a sacrificial hole scavenger increased the CO yield to over 65 mmol \bullet g $^{-1}$ but decreased the pinacol yield to 11 mmol \bullet g $^{-1}$ (Figure S46, Supporting Information). These results support the use of the photogenerated holes and electrons in CdS@PCN-Co for C–C coupling and CO2 reduction, respectively.

The significantly lower CO and pinacol selectivity of CdS@PCN over CdS@PCN-Co supports the role of the Co sites in CO₂ reduction and C–C coupling reaction. Furthermore, CdS@PCN-Co did not increase the H2 yield over CdS@PCN under Ar (Figure 4a), and CdS@PCN-Co showed a higher photocurrent under CO2 than under Ar, but CdS@PCN did not show similar photocurrents under CO₂ and Ar (Figure 4b). These results indicate that the Co sites facilitate electron-hole separation of CdS@PCN-Co for CO₂ reduction but not for H₂ evolution. CdS@PCN-Co, PCN-Co, and PCN showed stronger EPR signals under irradiation than in the dark, indicating the photogeneration of radicals in this photocatalytic system. CdS@PCN-Co showed stronger EPR signal intensity than PCN-Co and PCN, indicative of more efficient electron-hole separation in CdS@PCN-Co (Figure S49a,b, Supporting Information).[68] The EPR results are consistent with the photocurrent response results. Furthermore, CdS@PCN-Co showed stronger EPR signals under CO₂ than under Ar (Figure S49c, Supporting Information), suggesting the increased concentration of photogenerated holes due to the consumption of photogenerated electrons for CO2 reduction. However, with the addition of 1-phenylethanol under CO2, the EPR signals completely disappeared for CdS@PCN-Co but were retained for PCN-Co (Figure \$49d, Supporting Information). This result indicates that the accumulated holes on the surface of CdS were consumed by 1-phenylethanol. Thus, the holes are efficiently generated on CdS QDs under the CO₂ atmosphere with the assistance of Co sites, leading to an increase in the local concentration of carbon radical intermediates in the confined space for the C-C coupling reaction.

As shown in Figure 4d, the selectivity for the C–C coupling product gradually increased from 51.2% to 95.3% with the 1-phenylethanol concentration increased from 8 to 60 mm, indicating the promotion of C–C coupling at higher 1-phenylethanol concentrations (Figures S50 and S51, Supporting Information). At the same 1-phenylethanol concentration (60 mm), CdS@PCN-Co gave a much higher pinacol selectivity (96.2%) than CdS/PCN-Co (36.7%, Figure 4d). These results confirm the spatial confinement effect of MOFs, where the MOF micro-reactors enrich the substrates and radical intermediates for C–C coupling.

The influence of the confined environment of CdS@PCN-Co on the catalytic performance was further examined by in situ DRIFT spectroscopy and EPR measurements. As shown in Figure 4c, the characteristic peaks of COOH* at ≈1539, 1558, and 1653 cm⁻¹ and CO* at 2078 cm⁻¹ were observed. Notably,

15214095, 0, Downloaded from https://advanced.onlinelibrary.wiley.com/doi/10.1002/adma.202506133 by Tianjin University Of, Wiley Online Library on [1407/2025]. See the Terms and Conditions (https://onlinelibrary.wiley.com/term/terms/

onditions) on Wiley Online Library for rules of use; OA articles are governed by the applicable Creative Common

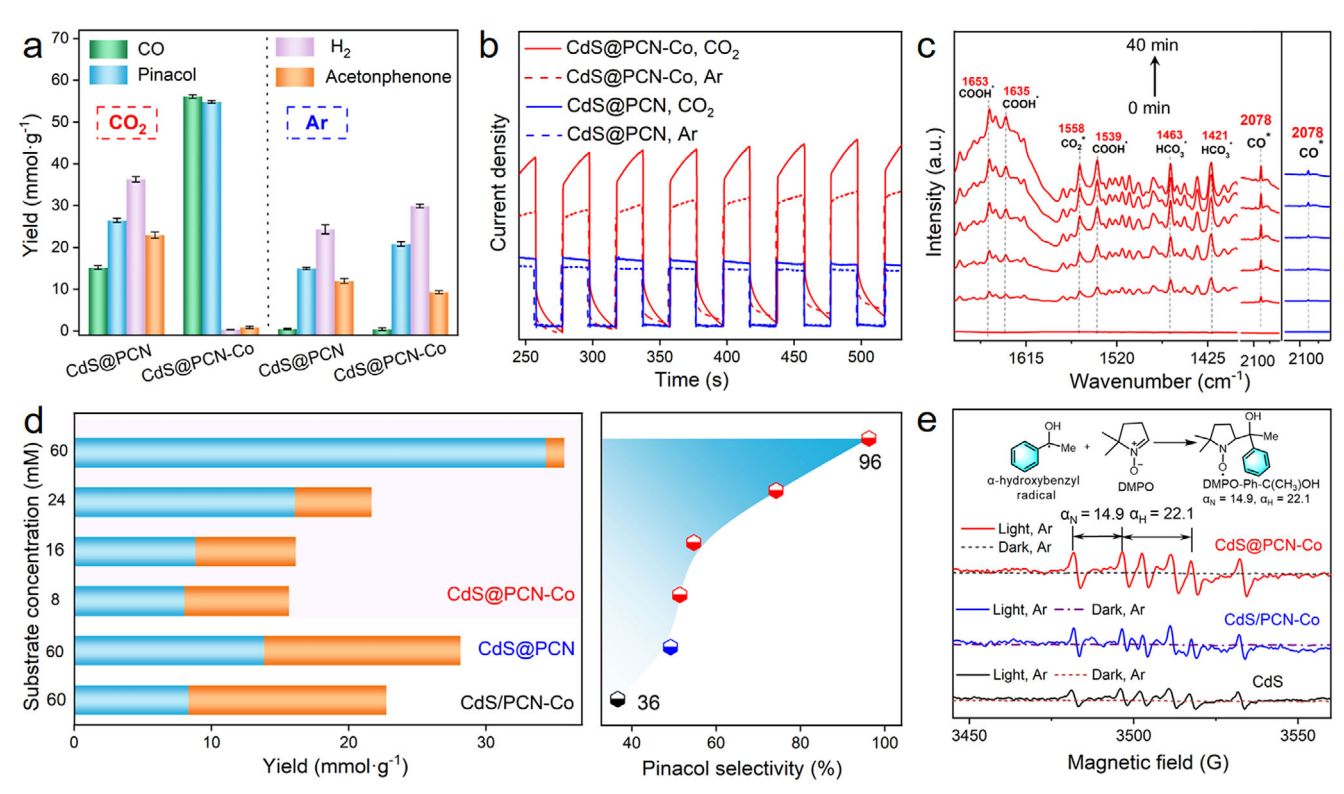


Figure 4. Reaction mechanism for CO_2 photoreduction and C–C coupling. a) Photocatalytic performance and b) photocurrent response of CdS@PCN and CdS@PCN-Co under Ar and CO_2 atmosphere, respectively. c) In situ diffuse reflectance infrared Fourier transform (DRIFT) spectroscopy over CdS@PCN-Co (red) and CdS/PCN-Co (blue) for CO_2 photoreduction with 1-phenylethanol. d) Photocatalytic performance and pinacol selectivity with different substrate concentrations in 6 h. e) EPR spectra of CdS, CdS/PCN-Co, and CdS@PCN-Co in the dark or under illumination of Ar-saturated acetonitrile solution of 5,5-dimethyl-1-pyrrolidine (DMPO) with 1-phenylethanol.

CdS@PCN-Co showed much higher intensity of the CO* peak at 2078 cm $^{-1}$ than CdS/PCN-Co (Figure 4c; Figure S52, Supporting Information), indicating a higher activity of CO $_2$ reduction for CdS@PCN-Co. In situ EPR was utilized to monitor the generation of α -hydroxybenzyl radical via C $_{\alpha$ -H bond cleavage in 1-phenylethanol. The DMPO was used to trap α -hydroxybenzyl radical. Under irradiation, the α -hydroxybenzyl-DMPO adduct was detected with the expected coupling constants of $\alpha_{\rm N}=14.9$ and $\alpha_{\rm H}=22.1.^{[69-71]}$ Notably, the EPR signal intensity for the α -hydroxybenzyl-DMPO adduct followed the order of CdS@PCN-Co > CdS/PCN-Co > CdS (Figure 4e), indicating the most efficient C–C coupling by CdS@PCN-Co.

IR spectroscopy was also used to investigate the interactions of 1-phenylethanol with the photocatalysts (Figure S53, Supporting Information). As shown in Figure S53c (Supporting Information), 1-phenylethanol showed the $\nu_{\text{C-O}}$ peak at 1038 cm $^{-1}$. The $\nu_{\text{C-O}}$ peaks of both CdS@PCN-Co/1-phenylethanol and PCN-Co/1-phenylethanol samples shifted to 1055 cm $^{-1}$ in the differential IR spectra, suggesting the interactions of 1-phenylethanol with the Zr $_6$ SBU via —C—OH—Zr— bonds. [72,73] The $\nu_{\text{C-O}}$ peak was not observed for CdS/1-phenylethanol, indicating weak adsorption of 1-phenylethanol on CdS. In addition, the $\nu_{\mu 3\text{-OH}}$ peak of the Zr $_6$ cluster shifted from 3672 to 3613 cm $^{-1}$, consistent with hydrogen bonding between μ_3 -OH in the Zr $_6$ cluster and the —OH group in 1-phenylethanol (Figure S53d, Supporting Information). $^{[63,64,74]}$ This interaction may also

inhibit dehydrogenation of the α -hydroxybenzyl radical to produce acetophenone. ^[75] Taken together, CdS@PCN-Co enriches 1-phenylethanol via absorption on the Zr₆ SBU to facilitate C–C coupling.

We performed density functional theory (DFT) calculations to assess the influence of Zr_6 SBU and CdS QDs on the Gibbs free energy changes (ΔG) for the formation of C–C coupling products. Four adsorption site models of Zr SBU*-CdS, Zr SBU*, CdS*-Zr SBU, and CdS* were constructed to compare the substrateadsorbing ability on different sites (Figure 5a). As shown in Figure 5b, the adsorption of 1-phenylethanol on Zr SBU*-CdS exhibited a more negative ΔG than the other three models. Both 1-phenylethanol and CdS are adsorbed on one Zr₆ SBU to facilitate 1-phenylethanol oxidation by the holes on the CdS surface. Consistent with the IR results, DFT calculations revealed hydrogen bonding between μ_3 -OH in the Zr_6 cluster and -OH in 1-phenylethanol. Furthermore, 1-phenylethanol was oxidized by the photogenerated holes to form α -hydroxybenzyl radicals at these adsorption sites. Similar ΔG values were observed for the dehydrogenation of 1-phenylethanol by Zr SBU*-CdS ($\Delta G =$ 1.924 eV) and Zr SBU* ($\Delta G = 1.838$ eV), which is lower than that by CdS QDs ($\Delta G = 2.187$ eV, Figure S54, Supporting Information). The ΔG values for the radical C–C coupling process was calculated to be -0.997 eV, which is more negative than that of the dehydrogenation of the O-H bond in α -hydroxybenzyl radicals to form acetophenone and H· (-0.794 eV, Table \$10, Supporting

15214095, 0, Downloaded from https://advanced.onlinelibrary.wiley.com/doi/10.1002/adma.202506133 by Tianjin University Of, Wiley Online Library on [14.07/2025]. See the Terms and Conditions (https://onlinelibrary.wiley.com/erms

-and-conditions) on Wiley Online Library for rules of use; OA articles are governed by the applicable Creative Commons

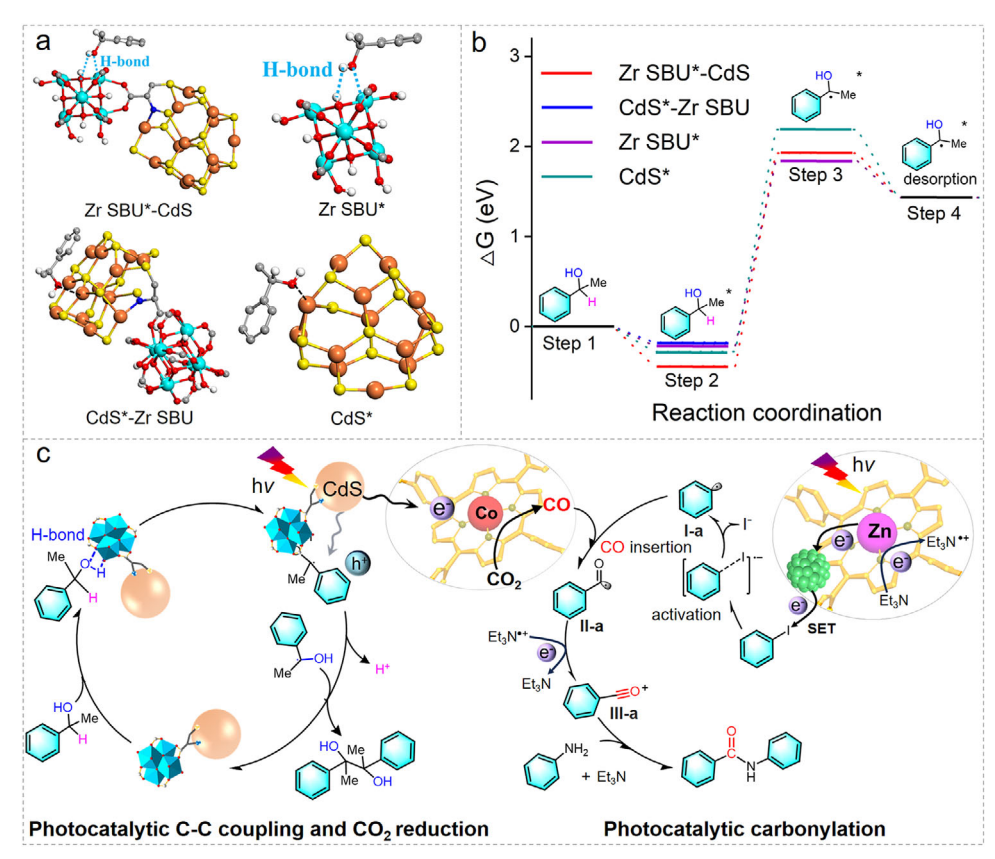


Figure 5. DFT calculations and proposed mechanism. a) DFT calculations for structural models of Zr SBU*-CdS, Zr SBU*, CdS*-Zr SBU and CdS*. b) Δ*G* for 1-phenylethanol deprotonation. c) Proposed mechanism for C–C coupling, CO₂ photoreduction, and carbonylation over CdS@PCN-Co and Pd/PCN-Zn.

Information). As a result, the adsorption site of Zr SBU*-CdS can facilitate dehydrogenation to produce α -hydroxybenzyl radicals, and the desorbed radicals undergo C–C coupling in the catalytic microenvironment.

Based on the aforementioned experiments and analysis, CdS in CdS@PCN-Co is capable of utilizing visible light to generate electron and hole pairs. The photogenerated electrons on CdS are efficiently captured by adjacent Co sites, leaving behind photogenerated holes on CdS. The reduced Co sites efficiently reduce CO₂ to CO, while the holes on CdS oxidize 1-phenylethanol to form α -hydroxybenzyl radicals which couple to form the pinacol product. In this photocatalytic system, aromatic alcohols and CO₂ are efficiently and selectively transformed into value-added chemicals (pinacol) and the important C1 source (CO, Figure 5c; Figures \$55, \$56, Notes \$1 and \$2, Supporting Information). This CO can be used for photocatalytic carbonylative reactions. The proposed mechanism for the carbonylative reaction has been illustrated in Figure 5c,^[76] supported by additional experiments and theoretical calculations (Figures S57–S61, Supporting Information).

The photocurrent response of Pd/PCN-Zn and PCN-Zn was performed in the presence of iodobenzene to track the electron transfer pathway.^[77] As shown in Figure S57 (Supporting Information), the photocurrent intensity of PCN-Zn did not show significant change before and after adding iodobenzene. In contrast, Pd/PCN-Zn exhibited a significantly weakened photocur-

rent signal after introducing iodobenzene. These results indicate the occurrence of photoinduced electron transfer from Pd clusters to iodobenzene, resulting in the formation of a transient negative ion species.^[78-81] DFT calculations indicated that the transfer of electrons to the unoccupied orbital of iodobenzene results in a significant increase in the C-I bond length from 0.216 to 0.310 nm (Figure S58, Supporting Information), which contributed to facilitating the cleavage of the C-I bond to afford phenyl radical. [81,82] Subsequently, the phenyl radicals undergo nucleophilic addition with CO to form a benzoyl radical intermediate.^[76] This intermediate transfers an electron to Et₃N^{•+}, yielding the acyl cation intermediate. This process was also rationalized by DFT calculations, where Path A is thermodynamically more favorable than Path B (Figure \$59, Supporting Information). Ultimately, the amine can react with the acyl cation, resulting in the formation of the target product. [83–85]

2.6. Continuous-Flow System for Tandem Photocatalysis

We developed a tandem photocatalytic system composed of two continuous-flow reactors, designated as A and B. CdS@PCN-Co and Pd/PCN-Zn were respectively immobilizing in the continuous-flow reactors A and B to integrate CO₂ photoreduction with photo-oxidative C–C coupling and photocatalytic carbonylation (**Figure 6**a; Figure S62, Supporting Information). In

15214095, 0, Downloaded from https://advanced.onlinelibrary.wiley.com/doi/10.1002/adma.202506133 by Tianjin University Of, Wiley Online Library on [1407/2025]. See the Terms and Conditions (https://onlinelibrary.wiley.com/term/terms/

onditions) on Wiley Online Library for rules of use; OA articles are governed by the applicable Creative Common

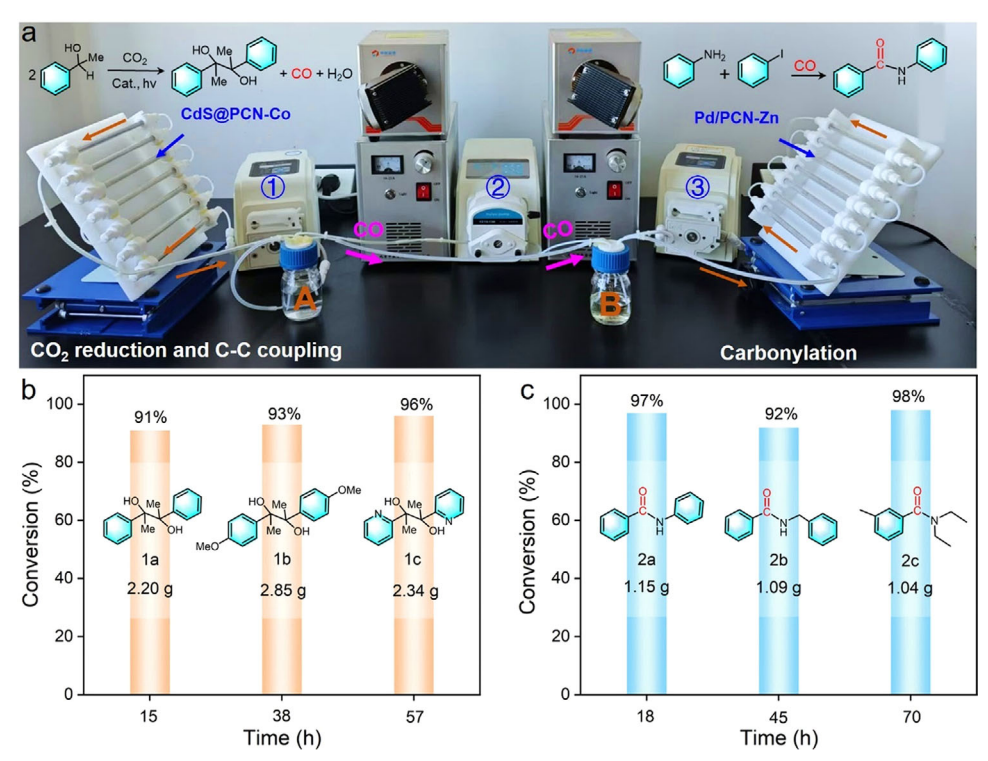


Figure 6. Gram-scale photosynthesis with a dual continuous-flow system. a) Photograph of the continuous-flow photoreactors. b) Long-term operation for C–C coupling and CO₂ photoreduction over CdS@PCN-Co. c) Long-term operation for carbonylation over Pd/PCN-Zn. Reaction conditions: reactor A: 150 mg of CdS@PCN-Co, 120 mL CH₃CN, 1-phenylethanol (20 mmol) and Na₂CO₃ (20 mmol), visible light ($\lambda \ge 400$ nm, 180 mW cm⁻²), under CO₂. Reactor B: 180 mg of Pd/PCN-Zn, 100 mL DMF, aryliodides (6 mmol), amine substrates (12 mmol), and TEA (30 mmol), visible light ($\lambda \ge 400$ nm, 150 mW cm⁻²).

reactor A, CdS@PCN-Co can efficiently drive C-C coupling and CO₂ reduction upon excitation with a Xenon lamp (>400 nm). Impressively, gram-scale photosynthesis of pinacol was achieved with efficient CO evolution. CO from reactor A can be directly pumped into reactor B and utilized as a C1 source for the gram-scale photosynthesis of benzanilide with high purity (97%). In photocatalyst-immobilized continuous-flow reactors, efficient gram-scale photosynthesis of diverse catalytic products was accomplished by conveniently substituting reaction vessels with those containing different substrates. Especially, for the first time, high-value commercial pesticide DTTE can be prepared via this protocol with a yield of 98% under mild conditions (Figure 6b,c). As a result, we successfully developed an efficient and sustainable catalytic system for the continuous co-production of fine chemicals via photochemical CO₂-to-CO reduction.

3. Conclusion

In this work, we have designed and synthesized two stable composites CdS@PCN-Co and Pd/PCN-Zn for tandem photocatalysis. CdS@PCN-Co can simultaneously drive CO $_2$ -to-CO conversion and C–C coupling. Pd/PCN-Zn was used for photocatalytic carbonylation reaction with CO as a C1 source. Subsequently, CdS@PCN-Co and Pd/PCN-Zn were immobilized in the continuous flow reactors A and B, respectively, to integrate CO $_2$ photoreduction with photo-oxidative C–C coupling and photo-

catalytic carbonylation. In reactor A, CdS@PCN-Co exhibits an excellent performance in CO_2 conversion and selective C–C coupling, resulting in gram-scale photosynthesis of pinacol and efficient CO evolution. CO from reactor A can be directly utilized as a C1 source in reactor B for the gram-scale photosynthesis of benzanilide and its derivatives with high purity (>90%). For the first time, gram-scale photosynthesis of the high-value commercial pesticide DTTE was successfully achieved under mild conditions, using CO_2 as a carbon source. Owing to its extremely high efficiency, ease of operation, and sustainable nature, this strategy for developing a continuous tandem photocatalytic system has significant potential for large-scale solar-driven CO_2 conversion in the near future.

Supporting Information

Supporting Information is available from the Wiley Online Library or from the author.

Acknowledgements

X.-L.M. and W.-X.S. contributed equally to this work. This work was financially supported by the National Natural Science Foundation of China (92461314, 22371207, and 22171209).

Conflict of Interest

The authors declare no conflict of interest.

15214095, 0, Downloaded from https://advanced.onlinelibrary.wiley.com/doi/10.1002/adma.202506133 by Tianjin University Of, Wiley Online Library on [1407/2025]. See the Terms

and Conditions (https://onlinelibrary.wiley.com/term

nditions) on Wiley Online Library for rules of use; OA articles are governed by the applicable Creative Con

Data Availability Statement

The data that support the findings of this study are available from the corresponding author upon reasonable request.

Keywords

CO₂-to-CO conversion, metal–organic frameworks, synergistic catalysis

Received: April 1, 2025 Revised: June 7, 2025 Published online:

- Z. Guo, G. Chen, C. Cometto, B. Ma, H. Zhao, T. Groizard, L. Chen, H. Fan, W.-L. Man, S.-M. Yiu, K.-C. Lau, T.-C. Lau, M. Robert, Nat. Catal. 2019, 2, 801.
- [2] Y. Jiao, Y. Zheng, M. Jaroniec, S. Z. Qiao, Chem. Soc. Rev. 2015, 44, 2060.
- [3] D. U. Nielsen, X.-M. Hu, K. Daasbjerg, T. Skrydstrup, *Nat. Catal.* 2018, 1, 244.
- [4] X. Jiao, K. Zheng, L. Liang, X. Li, Y. Sun, Y. Xie, Chem. Soc. Rev. 2020, 49, 6592.
- [5] Y. Yamazaki, M. Miyaji, O. Ishitani, J. Am. Chem. Soc. 2022, 144, 6640.
- [6] M. Aresta, A. Dibenedetto, A. Angelini, Chem. Rev. 2014, 114, 1709.
- [7] J. Li, H. Huang, W. Xue, K. Sun, X. Song, C. Wu, L. Nie, Y. Li, C. Liu, Y. Pan, H.-L. Jiang, D. Mei, C. Zhong, Nat. Catal. 2021, 4, 719.
- [8] Z. Jiang, X. Xu, Y. Ma, H. S. Cho, D. Ding, C. Wang, J. Wu, P. Oleynikov, M. Jia, J. Cheng, Y. Zhou, O. Terasaki, T. Peng, L. Zan, H. Deng, *Nature* 2020, 586, 549.
- [9] E. Nikoloudakis, I. Lopez-Duarte, G. Charalambidis, K. Ladomenou, M. Ince, A. G. Coutsolelos, *Chem. Soc. Rev.* 2022, *51*, 6965.
- [10] M. G. Lee, X.-Y. Li, A. Ozden, J. Wicks, P. Ou, Y. Li, R. Dorakhan, J. Lee, H. K. Park, J. W. Yang, B. Chen, J. Abed, R. dos Reis, G. Lee, J. E. Huang, T. Peng, Y.-H. Chin, D. Sinton, E. H. Sargent, *Nat. Catal.* 2023, 6, 310.
- [11] M. Liu, Q. Wang, T. Luo, M. Herran, X. Cao, W. Liao, L. Zhu, H. Li, A. Stefancu, Y.-R. Lu, T.-S. Chan, E. Pensa, C. Ma, S. Zhang, R. Xiao, E. Cortés, J. Am. Chem. Soc. 2024, 146, 468.
- [12] P. M. Stanley, V. Ramm, R. A. Fischer, J. Warnan, Nat. Synth 2024, 3, 307
- [13] Y. Wang, X. Shang, J. Shen, Z. Zhang, D. Wang, J. Lin, J. C. S. Wu, X. Fu, X. Wang, C. Li, Nat. Commun. 2020, 11, 3043.
- [14] A. Wagner, C. D. Sahm, E. Reisner, Nat. Catal. 2020, 3, 775.
- [15] C. Hepburn, E. Adlen, J. Beddington, E. A. Carter, S. Fuss, N. M. Dowell, J. C. Minx, P. Smith, C. K. Williams, *Nature* 2019, 575, 87.
- [16] K. Sun, Y. Huang, F. Sun, Q. Wang, Y. Zhou, J. Wang, Q. Zhang, X. Zheng, F. Fan, Y. Luo, J. Jiang, H.-L. Jiang, Nat. Chem. 2024, 16, 1638.
- [17] B. Song, W. Song, Y. Liang, Y. Liu, B. Li, H. Li, L. Zhang, Y. Ma, R. Ye, B. Z. Tang, D. Zhao, Y. Zhou, B. Liu, Angew. Chem., Int. Ed. 2025, 64, 202421248.
- [18] Z. K. Xin, Y. J. Gao, Y. Gao, H. W. Song, J. Zhao, F. Fan, A. D. Xia, X. B. Li, C. H. Tung, L. Z. Wu, Adv. Mater. 2022, 34, 2106662.
- [19] Y. Zhang, B. Johannessen, P. Zhang, J. Gong, J. Ran, S. Z. Qiao, Adv. Mater. 2023, 35, 2306923.
- [20] Y. Qu, X. Duan, Chem. Soc. Rev. 2013, 42, 2568.
- [21] Y. Zhao, G. I. N. Waterhouse, G. Chen, X. Xiong, L.-Z. Wu, C.-H. Tung, T. Zhang, Chem. Soc. Rev. 2019, 48, 1972.
- [22] W. Lyu, Y. Liu, D. Chen, F. Wang, Y. Li, Nat. Commun. 2024, 15, 10589.
- [23] A. Bavykina, N. Kolobov, I. S. Khan, J. A. Bau, A. Ramirez, J. Gascon, Chem. Rev. 2020, 120, 8468.

- [24] Y.-S. Xia, L. Zhang, J.-N. Lu, X.-H. Zhao, L.-Z. Dong, J. Liu, Y.-Q. Lan, Nat. Synth 2024, 3, 406.
- [25] Z. B. Fang, T. T. Liu, J. Liu, S. Jin, X. P. Wu, X. Q. Gong, K. Wang, Q. Yin, T. F. Liu, R. Cao, H. C. Zhou, J. Am. Chem. Soc. 2020, 142, 12515.
- [26] S. Dutta, A. Gurumoorthi, S. Lee, S. W. Jang, N. Kumari, Y. R. Hong, W. Choi, C. Y. Son, I. S. Lee, *Angew. Chem., Int. Ed.* 2023, 62, 202303890.
- [27] Y. Qin, Z. Li, Y. Duan, J. Guo, M. Zhao, Z. Tang, Matter 2022, 5, 3260.
- [28] C. S. Diercks, Y. Liu, K. E. Cordova, O. M. Yaghi, Nat. Mater. 2018, 17, 301.
- [29] P. J. Milner, R. L. Siegelman, A. C. Forse, M. I. Gonzalez, T. Runcevski, J. D. Martell, J. A. Reimer, J. R. Long, J. Am. Chem. Soc. 2017, 139, 13541.
- [30] B. An, Z. Li, Y. Song, J. Zhang, L. Zeng, C. Wang, W. Lin, Nat. Catal. 2019. 2, 709.
- [31] Y. Zhao, H. Zeng, X. W. Zhu, W. Lu, D. Li, Chem. Soc. Rev. 2021, 50, 4484.
- [32] S. Daliran, A. R. Oveisi, Y. Peng, A. López-Magano, M. Khajeh, R. Mas-Ballesté, J. Alemán, R. Luque, H. Garcia, Chem. Soc. Rev. 2022, 51, 7810.
- [33] K. I. Hadjiivanov, D. A. Panayotov, M. Y. Mihaylov, E. Z. Ivanova, K. K. Chakarova, S. M. Andonova, N. L. Drenchev, *Chem. Rev.* 2021, 121, 1286.
- [34] R. F. Mendes, F. Figueira, J. P. Leite, L. Gales, F. A. Almeida Paz, Chem. Soc. Rev. 2020, 49, 9121.
- [35] Q. Wang, D. Astruc, Chem. Rev. 2020, 120, 1438.
- [36] Y. Wang, N. Y. Huang, J. Q. Shen, P. Q. Liao, X. M. Chen, J. P. Zhang, J. Am. Chem. Soc. 2018, 140, 38.
- [37] T.-C. Zhuo, Y. Song, G.-L. Zhuang, L.-P. Chang, S. Yao, W. Zhang, Y. Wang, P. Wang, W. Lin, T.-B. Lu, Z.-M. Zhang, J. Am. Chem. Soc. 2021, 143, 6114.
- [38] L. Y. Wu, Y. F. Mu, X. X. Guo, W. Zhang, Z. M. Zhang, M. Zhang, T. B. Lu, Angew. Chem., Int. Ed. 2019, 58, 9491.
- [39] S. Guo, L. H. Kong, P. Wang, S. Yao, T. B. Lu, Z. M. Zhang, Angew. Chem., Int. Ed. 2022, 61, 202206193.
- [40] Z. W. Huang, K. Q. Hu, X. B. Li, Z. N. Bin, Q. Y. Wu, Z. H. Zhang, Z. J. Guo, W. S. Wu, Z. F. Chai, L. Mei, W. Q. Shi, J. Am. Chem. Soc. 2023, 145, 18148
- [41] H.-Q. Yin, Z.-M. Zhang, T.-B. Lu, Acc. Chem. Res. 2023, 56, 2676.
- [42] G. Tian, Z. Li, C. Zhang, X. Liu, X. Fan, K. Shen, H. Meng, N. Wang, H. Xiong, M. Zhao, X. Liang, L. Luo, L. Zhang, B. Yan, X. Chen, H.-J. Peng, F. Wei, Nat. Commun. 2024, 15, 3037.
- [43] J. Ding, H. Bin Yang, X.-L. Ma, S. Liu, W. Liu, Q. Mao, Y. Huang, J. Li, T. Zhang, B. Liu, Nat. Energy 2023, 8, 1386.
- [44] Y. Hao, Y. L. Lu, Z. Jiao, C. Y. Su, Angew. Chem., Int. Ed. 2024, 63, 202317808.
- [45] H.-G. Jin, P.-C. Zhao, Y. Qian, J.-D. Xiao, Z.-S. Chao, H.-L. Jiang, Chem. Soc. Rev. 2024, 53, 9378.
- [46] T. Luo, L. Li, Y. Chen, J. An, C. Liu, Z. Yan, J. H. Carter, X. Han, A. M. Sheveleva, F. Tuna, E. J. L. McInnes, C. C. Tang, M. Schroder, S. Yang, Nat. Commun. 2021, 12, 3583.
- [47] M. Bonchio, J. Bonin, O. Ishitani, T.-B. Lu, T. Morikawa, A. J. Morris, E. Reisner, D. Sarkar, F. M. Toma, M. Robert, Nat. Catal. 2023, 6, 657.
- [48] J. Cao, Z.-J. Zheng, Z. Xu, L.-W. Xu, Coord. Chem. Rev. 2017, 336, 43.
- [49] P. Gotico, A. Del Vecchio, D. Audisio, A. Quaranta, Z. Halime, W. Leibl, A. Aukauloo, ChemPhotoChem 2018, 2, 715.
- [50] X. He, Y. Cao, X. D. Lang, N. Wang, L. N. He, ChemSusChem 2018, 11, 3382.
- [51] L. Ponsard, E. Nicolas, N. H. Tran, S. Lamaison, D. Wakerley, T. Cantat, M. Fontecave, ChemSusChem 2021, 14, 2198.
- [52] C. Lescot, D. U. Nielsen, I. S. Makarov, A. T. Lindhardt, K. Daasbjerg, T. Skrydstrup, J. Am. Chem. Soc. 2014, 136, 6142.
- [53] M. T. Jensen, M. H. Rønne, A. K. Ravn, R. W. Juhl, D. U. Nielsen, X.-M. Hu, S. U. Pedersen, K. Daasbjerg, T. Skrydstrup, *Nat. Commun.* 2017, 8, 489.



www.advancedsciencenews.com

ADVANCED MATERIALS

www.advmat.de

.5214095, 0, Downloaded from https://advanced.onlinelibrary.wiley.com/doi/10.1002/adma.202506133 by Tianjin University Of, Wiley Online Library on [14.07/2025]. See

the Terms

and Conditions (https://onlinelibrary.wiley

iditions) on Wiley Online Library for rules

of use; OA articles

are governed by the applicable Creative Con

- [54] S. Monticelli, A. Talbot, P. Gotico, F. Caillé, O. Loreau, A. Del Vecchio, A. Malandain, A. Sallustrau, W. Leibl, A. Aukauloo, F. Taran, Z. Halime, D. Audisio, *Nat. Commun.* 2023, 14, 4451.
- [55] R. Sang, Y. Hu, R. Razzaq, G. Mollaert, H. Atia, U. Bentrup, M. Sharif, H. Neumann, H. Junge, R. Jackstell, B. U. W. Maes, M. Beller, *Nat. Commun.* 2022, 13, 4432.
- [56] W. Zheng, X. Yang, Z. Li, B. Yang, Q. Zhang, L. Lei, Y. Hou, Angew. Chem., Int. Ed. 2023, 62, 202307283.
- [57] M. B. Ibrahim, R. Suleiman, M. Fettouhi, B. El Ali, RSC Adv. 2016, 6, 78826.
- [58] A. M. Sheta, S. Fernández, C. Liu, G. C. Dubed-Bandomo, J. Lloret-Fillol, Angew. Chem., Int. Ed. 2024, 63, 202403674.
- [59] Y. S. Xia, M. Tang, L. Zhang, J. Liu, C. Jiang, G. K. Gao, L. Z. Dong, L. G. Xie, Y. Q. Lan, Nat. Commun. 2022, 13, 2964.
- [60] S. Fu, S. Yao, S. Guo, G. C. Guo, W. Yuan, T. B. Lu, Z. M. Zhang, J. Am. Chem. Soc. 2021, 143, 20792.
- [61] D. W. Feng, Z. Y. Gu, J. R. Li, H. L. Jiang, Z. W. Wei, H. C. Zhou, Angew. Chem., Int. Ed. 2012, 51, 10307.
- [62] Q. Guo, F. Liang, X. B. Li, Y. J. Gao, M. Y. Huang, Y. Wang, S. G. Xia, X. Y. Gao, Q. C. Gan, Z. S. Lin, C. H. Tung, L. Z. Wu, *Chem* 2019, 5, 2605.
- [63] Q. Mo, L. Zhang, S. Li, H. Song, Y. Fan, C. Y. Su, J. Am. Chem. Soc. 2022, 144, 22747.
- [64] C. Koschnick, R. Staglich, T. Scholz, M. W. Terban, A. von Mankowski, G. Savasci, F. Binder, A. Schokel, M. Etter, J. Nuss, R. Siegel, L. S. Germann, C. Ochsenfeld, R. E. Dinnebier, J. Senker, B. V. Lotsch, *Nat. Commun.* 2021, 12, 3099.
- [65] F. Wang, T. Hou, X. Zhao, W. Yao, R. Fang, K. Shen, Y. Li, Adv. Mater. 2021, 33, 2102690.
- [66] X. Y. Lin, Y. H. Li, M. Y. Qi, Z. R. Tang, H. L. Jiang, Y. J. Xu, Nanoscale Horiz. 2020. 5, 714.
- [67] Z. Lin, Z. M. Zhang, Y. S. Chen, W. Lin, Angew. Chem., Int. Ed. 2016, 128, 13943

- [68] M. Xu, D. Li, K. Sun, L. Jiao, C. Xie, C. Ding, H. L. Jiang, Angew. Chem., Int. Ed. 2021, 60, 16372.
- [69] S. Xie, Z. Shen, J. Deng, P. Guo, Q. Zhang, H. Zhang, C. Ma, Z. Jiang, J. Cheng, D. Deng, Y. Wang, Nat. Commun. 2018, 9, 1181.
- [70] J. Y. Zeng, X. S. Wang, B. R. Xie, Q. R. Li, X. Z. Zhang, J. Am. Chem. Soc. 2022, 144, 1218.
- [71] L. Liu, R. M. Ward, J. M. Schomaker, Chem. Rev. 2019, 119, 12422.
- [72] P. Zhou, Q. Zhang, Y. Chao, L. Wang, Y. Li, H. Chen, L. Gu, S. Guo, Chem 2021, 7, 1033.
- [73] N. Planas, J. E. Mondloch, S. Tussupbayev, J. Borycz, L. Gagliardi, J. T. Hupp, O. K. Farha, C. J. Cramer, J. Phys. Chem. Lett. 2014, 5, 3716.
- [74] C. D. Wu, M. Zhao, Adv. Mater. 2017, 29, 1605446.
- [75] M. Hao, Y. Qin, J. Shen, B. Wang, Z. Li, ACS Catal. 2022, 12, 15282.
- [76] X. Liu, B. S. Portela, A. Wiedenbeck, C. H. Chrisman, R. S. Paton, G. M. Miyake, Angew. Chem., Int. Ed. 2024, 63, 202410928.
- [77] Q. Shen, J. Chen, X. Jing, C. Duan, Angew. Chem., Int. Ed. 2025, 137, 202506277.
- [78] T. Dohi, E. E. Elboray, K. Kikushima, K. Morimoto, Y. Kita, Chem. Rev. 2025, 125, 3440.
- [79] J. D. Nguyen, E. M. D'Amato, J. M. R. Narayanam, C. R. J. Stephenson, Nat. Chem. 2012, 4, 854.
- [80] F. Wang, C. Li, H. Chen, R. Jiang, L.-D. Sun, Q. Li, J. Wang, J. C. Yu, C.-H. Yan, J. Am. Chem. Soc. 2013, 135, 5588.
- [81] I. Ghosh, L. Marzo, A. Das, R. Shaikh, B. König, Acc. Chem. Res. 2016, 49, 1566.
- [82] I. Ghosh, T. Ghosh, J. I. Bardagi, B. König, Science 2014, 346, 725.
- [83] W. Guo, L. Q. Lu, Y. Wang, Y. N. Wang, J. R. Chen, W. J. Xiao, Angew. Chem., Int. Ed. 2014, 54, 2265.
- [84] M. Majek, A. Jacobi von Wangelin, Angew. Chem., Int. Ed. 2015, 54, 2270
- [85] L.-C. Wang, X.-F. Wu, Acc. Chem. Res. 2025, 58, 1036.